Separation Science and Technology
Publication details, including instructions for authors and subscription information:
http://www.informaworld.com/smpp/title~content=t713708471

Retention Characteristics of Time-Delayed Exponential Field-Programmed Sedimentation Field-Flow Fractionation

W. W. Yau[a]; J. J. Kirkland[a]
[a] CENTRAL RESEARCH AND DEVELOPMENT DEPARTMENT, EXPERIMENTAL STATION E. I. DU PONT DE NEMOURS & CO. WILMINGTON, DELAWARE

To cite this Article Yau, W. W. and Kirkland, J. J.(1981) 'Retention Characteristics of Time-Delayed Exponential Field-Programmed Sedimentation Field-Flow Fractionation', Separation Science and Technology, 16: 6, 577 — 605
To link to this Article: DOI: 10.1080/01496398108058118
URL: http://dx.doi.org/10.1080/01496398108058118

SEPARATION SCIENCE AND TECHNOLOGY, 16(6), pp. 577-605, 1981

Retention Characteristics of Time-Delayed Exponential Field-Programmed Sedimentation Field-Flow Fractionation

W. W. YAU and J. J. KIRKLAND

CENTRAL RESEARCH AND DEVELOPMENT DEPARTMENT
EXPERIMENTAL STATION
E. I. DU PONT DE NEMOURS & CO.
WILMINGTON, DELAWARE 19898

ABSTRACT

Sedimentation field-flow fractionation (SFFF) is a promising method for the high-resolution separation of a wide variety of suspended particulates and dissolved macromolecules. By using a new SFFF technique with a time-delayed exponential force-field (rotor speed) decay, quantitative particle-size distribution analyses in the 0.01-1 μm range can be performed in a few minutes. Relative to constant-field SFFF, programmed force-field operation can drastically decrease analysis time and improve detection sensitivity while maintaining adequate resolution. The linear relationship between particle retention and logarithm of particle diameter or mass for the new technique significantly simplifies data handling for convenient and accurate analyses. Standard graphs have been prepared to show how separation variables such as exponential decay time constant, τ, initial rotor speed, ω_o, channel thickness, W, and flowrate, F, can affect particle retention. These simple and quantitative relationships are useful for designing efficient SFFF separations. Conversion of raw data to actual particle size distributions involves negligible errors because the accuracy of SFFF analyses is not significantly affected by instrumental band broadening. The concepts of specific SFFF resolution and particle discrimination factors are introduced to permit the comparison of SFFF resolution with other separation techniques.

INTRODUCTION

High-resolution separation of a wide range of particulates and soluble macromolecules can be made by sedimentation field-flow fractionation (SFFF). This "one-phase chromatography" method involves a very thin, open channel, and sample retention is obtained because of the redistribution of components from fast- to slow-moving mobile-phase streams under the influence of an external centrifugal force. The background and theory of constant-field (or constant-rotor-speed) SFFF has previously been described by Giddings et al. (1-3). Recently, we introduced the concept of simple exponential field-programmed SFFF to reduce separation time and improve particle detectability (4). This paper describes the theory and operation of a new method of time-delayed exponential field-programmed SFFF, or TDE-SFFF for short. This TDE-SFFF method shows significant advantages over the simple exponential SFFF approach, most importantly, in increased accuracy and convenience of interpreting SFFF data in particle-size analyses. This new approach also produces highly predictable retention data, which are useful for obtaining accurate particle-size distribution analyses in the particle size range of 0.01-1 μm.

Reducing the force field during SFFF separations causes normally highly retained large particles to elute earlier and with less band dispersion than those from constant-field separations. However, since the force field directly affects retention, the type of field programming also directly determines particle size dependence and the interpretive aspects of SFFF retention. Therefore, a practical SFFF method also should have simple and predictable particle retention characteristics for convenient and accurate data interpretation. This paper shows the advantages of a particular form of field programming that produces a log-linear relationship between particle retention and particle size. Such an approach achieves a simple linear dependence between particle retention and logarithm of particle diameter (or particle mass).

Our previous work indicated that an approximation to the desired retention characteristics can be obtained by simple exponential field decay programming (4). Our theoretical analysis now shows that a much improved force field programming involves a unique form: exponential force field decay following a particular time-delay. In actual practice, this TDE-SFFF scheme involves holding an initial high level of force field constant for a predetermined time of τ minutes. The field is then allowed to decay exponentially with a decay time constant also of τ minutes. According to this theory, the matching of the delay and decay time constants assures the exact linear relationship between SFFF retention and the logarithm of sample particle size.

The fact that particle retention in TDE-SFFF has the same log-linear functional dependence on both particle diameter and particle mass is uniquely desirable for interpreting SFFF data. With this approach, both sample particle size distribution and molecular weight distribution are obtainable from the same fractogram. Another important feature of TDE-SFFF is that the dependence of particle retention on determinable separation parameters is highly predictable. These simple and quantitative predictions are very useful for designing and controlling SFFF separations. The log-linear retention relationship also lends itself to a simple interpretation of the effect of instrumental band broadening on the accuracy of particle size analysis. Resolution calculations based on experimental data confirm that SFFF is a very high resolution technique, with negligible effect of band broadening on the accuracy of particle-size analyses.

GENERAL THEORY

Successful SFFF separations of particles by size or mass have previously been demonstrated (1-4). Observed particle retention at constant field can be quantitatively described by simple equilibrium theory (1):

$$t_R \approx \left(\frac{V_o WG\Delta\rho}{6R_o TF\rho_s}\right) \cdot M \approx \left(\frac{\pi V_o WG\Delta\rho}{36kTF}\right) \cdot d_p^3 \quad (1)$$

where, t_R = solute or particle peak retention time (min); V_o = channel void volume (cm^3); W = channel thickness (cm); G = centrifugal force field (cm/S^2); $\Delta\rho$ = density difference between sample component and mobile phase (g/cm^3); R_o = gas constant (8.31×10^7 $g.cm^2/S^2.deg.mol$); T = absolute temperature (Kelvin); F = volumetric flowrate of carrier liquid mobile phase (cm^3/min); ρ_s = density of dispersed particles or solvated macromolecules (g/cm^3); M = molecular weight of solvated macromolecules, or particle mass of colloid dispersion (g/mol); k = Boltzmann constant (1.38×10^{-16} $g.cm^2/S^2.deg$); and d_p = particle diameter (diameter of an equivalent sphere, cm). In this case,

$$G = \omega_R^2 r, \quad (2)$$

or

$$G = (\pi\omega/30)^2 r \quad (2a)$$

where, ω_R = centrifuge speed (rad/s), ω = centrifuge speed (rpm), and r = radial distance from centrifuge rotating axis to SFFF channel.

While constant field experiments are useful for demonstrating the fundamental features of SFFF separations, there are many practical limitations of using this form of SFFF for actual analysis of sample particle size. Equation 1 shows that SFFF retention in a constant field is linearly proportioned to particle mass. However, dependence of SFFF retention on particle size is highly non-linear (cubic dependency), and this relationship is inconvenient for transforming SFFF fractograms to actual sample particle-size distribution. The fact that constant-field SFFF separations also suffer from a non-linear particle size-resolution or particle-size separation power across a SFFF fractogram is illustrated in Figure 1. Here, a mixture of polystyrene latex standards is fractionated with two different levels of centrifugal force fields. The non-uniform resolution of particles is obvious; larger parti-

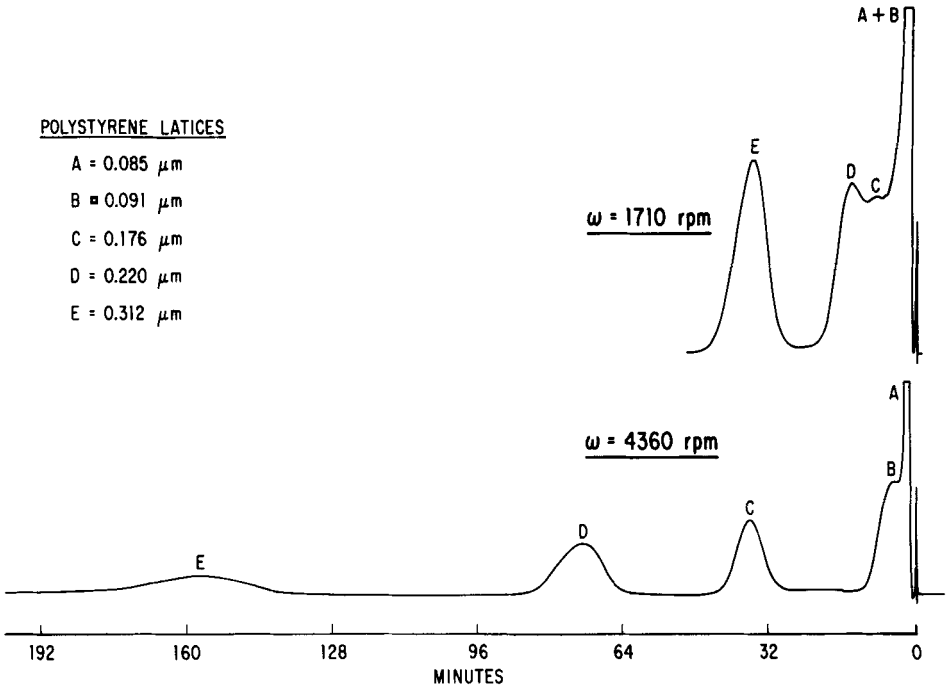

FIGURE 1. Effect of Rotor Speed in Constant-Field SFFF. Channel, 57 × 2.54 × 0.0254 cm; mobile phase, 0.1% FL 70; flowrate, 2.0 ml/min.; relaxation, 10.0 min at ω; sample 25 μL of 0.1% 0.085 μm, 0.09% 0.091 μm; 0.04% ea. of 0.176, 0.220, 0.312 μm polystyrene latex standards; detector, UV, 300 nm; temperature, 22°C.

cles in both fractograms are resolved much better than smaller particles. In the lower force field experiment (ω = 1,710 rpm), only the largest particle component of the sample mixture is completely resolved from a group of four unresolved smaller particles. At the higher field (ω = 4,360 rpm), the larger particles are excessively resolved at long retention times; however, the two smaller particle components still overlap. Therefore, with constant-field SFFF, the gain in resolution at higher force fields is obtained at the expense of long analysis times and excessive band broadening of late eluting peaks. Separations of peaks with continuously increasing band widths also cause detection problems.

Detector sensitivity appropriate for sharper, early eluting peaks often is not sufficient for detecting the low particle concentrations associated with highly dispersed, late-eluting peaks.

To solve the inherent problems of both the long analysis times and the poor detectability of the late-eluting peaks in constant-field SFFF separations, Giddings et al. used decreasing force fields, including stepwise, linear decay, and parabolic decay field programming (1,2,3). Although both analysis time and sample detectability were improved, such programming schemes inadvertently complicate the quantitative relationships between retention and particle mass or particle size. The simple retention-mass relationship of constant field SFFF is sacrificed.

For optimum utility, field programming in SFFF should also provide simple and predictable retention characteristics. We originally proposed a simple exponential force-field decay to obtain an approximate log-linear relationship between SFFF retention and particle mass and size (4). The current work refines this method by introducing a unique time-delayed constant-field component, followed by an exponential field decay. This new approach produces more accurate correlation between the logarithm of particle size and SFFF retention time. In addition, it provides the advantages of versatility and convenience in optimizing and manipulating separation range and resolution. In TDE-SFFF, retention characteristics are analogous to those of size-exclusion chromatography (SEC), and many of the highly developed data-handling techniques and resolution-accuracy concepts in SEC (5) can be readily adopted for use in SFFF particle-size distribution analyses.

Constant Field SFFF

Giddings et al. (1) have shown that in constant-field SFFF the average migration rate of retained sample components is smaller than the average linear velocity of the liquid carrier or mobile phase by a factor R, the retention ratio:

$$R = V_p/\langle v\rangle \tag{3}$$

$$R = 6\lambda\left[\coth\ \frac{1}{2\lambda}\ - 2\lambda\right] \tag{4}$$

where

$$\lambda = \frac{\ell}{W} = \frac{R_o T}{MGW(\Delta\rho/\rho_s)} = \frac{6kT}{\pi d_p^{\,3} GW\Delta\rho} \tag{5}$$

R = retention ratio (dimensionless); coth(1/2λ) = hyperbolic cotangent of (1/2λ); λ = a dimensionless retention parameter; ℓ = characteristic particle layer thickness (cm) under a particular force field; V_p = linear velocity of particle migration (cm/S); <v> = average mobile phase velocity (cm/S); and, the other symbols as previously defined. For highly retained sample components, simplifying approximations to Equation 4 are possible:

$$R \cong 6\lambda - 12\lambda^2 \qquad \text{(for } R<0.7\text{)} \tag{6}$$

or

$$R \cong 6\lambda \qquad \text{(for } R<0.3\text{)} \tag{7}$$

Figure 2 shows the close approximation of calculated R and λ curves from Equations 6 and 7, compared to that of Equation 4 at small R values.

In constant-field SFFF, a sample component migrates with a constant average linear velocity of R<v> or V_p. The retention time of a highly retained component is expected to increase in proportion to particle mass (1):

$$t_R = \frac{L}{R\langle v\rangle} \cong \frac{t_o}{6\lambda} \tag{8}$$

or,

$$t_R \cong \frac{t_o MGW(\Delta\rho/\rho_s)}{6R_o T} = \frac{t_o \pi d_p^{\,3} GW\Delta\rho}{36kT} \tag{9}$$

where L = length of the SFFF channel (cm) and t_o = the retention time of the solvent peak. Note that Equation 9 is identical to Equation 1, since $t_o = V_o/F$.

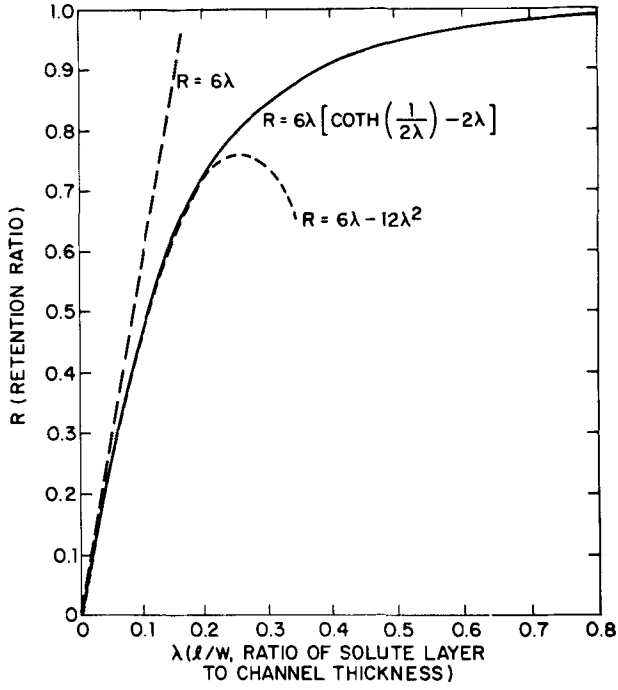

FIGURE 2. Theoretical R versus λ Plot for FFF Retention.

Time Delayed Exponential SFFF (TDE-SFFF)

In field-programmed SFFF, the retention ratio R becomes a function of time, depending on the particular field strength at that time:

$$L = \int_{o}^{t_R} R(t) \quad \langle v \rangle dt \tag{10}$$

In this case, the time-dependent retention ratio R(t) is still expressed by Equations 1-3, except that force field G is now a time-dependent function (i.e., G = G(t)).

To achieve the desired log-linear relationship between SFFF retention and particle size, we have developed a more general retention expression that describes the retention resulting from a combined SFFF sequence consisting of constant field operation

followed by an exponential field decay. A general form of this time-delayed exponential-decay force field programming is:

$$G(t) = G_o \qquad (t \leq \chi) \tag{11}$$

$$G(t) = G_o e^{-(t-\chi)/\tau} \qquad (t > \chi) \tag{12}$$

where G_o = initial sedimentation force field (cm/sec^2); τ = the exponential-decay time constant (min); and χ = an arbitrary delay time (min). SFFF retention obtained under this sequence can be predicted by substituting Equations 11 and 12 into Equation 10 and integrating to obtain:

for $t \leq \chi$,

$$L = \frac{6\emptyset}{M} \langle v \rangle t \tag{13}$$

and, for $t > \chi$,

$$L = \frac{6\emptyset}{M} \langle v \rangle \left[\int_o^{\chi} dt + \int_{\chi}^{t_R} e^{-(t-\chi)/\tau} dt \right]$$

$$= \frac{6\emptyset}{M} \langle v \rangle \left[\chi + \tau e^{(t_R-\chi)/\tau} - \tau \right] \tag{14}$$

where

$$\emptyset = \frac{R_o T}{G_o W(\Delta\rho/\rho_s)} \tag{15}$$

Note that when $\chi = 0$, Equations 13 and 14 reduce to the case of the simple (no time-delay) exponential-decay (4) that gives approximate log-linear SFFF retention characteristics. But more importantly, an exact log-linear SFFF retention relationship can be predicted for $t_R > \tau$ by allowing χ to equal τ in Equations 13 and 14. Under these unique conditions, the theory predicts true log-linear SFFF retentions. In this preferred TDE-SFFF, mobile phase flow is initiated after sample injection, while the initial force field G_o is maintained for a time equal to time τ, prior to force field decay. After time τ the force field is allowed to decay exponentially, also with a time constant τ. In this situation:

for $t \leq \tau$, $G = G_o$ (16)

$$M = 6\emptyset(t_R/t_o) \quad (17)$$

for $t > \tau$,

$$G = G_o e^{-(t-\tau)/\tau} \quad (18)$$

$$M = 6\emptyset \left(\frac{\tau}{et_o} \right) e^{t_R/\tau} \quad (19)$$

Equation 19 can be written in logarithm form:

$$\ln M = \ln \alpha + t_R/\tau \quad (20)$$

or

$$\ln d_p = \ln \beta + t_R/3\tau \quad (21)$$

where

$$\alpha = \frac{6R_o T\tau}{et_o G_o W(\Delta\rho/\rho_s)} \quad (22)$$

and

$$\beta = \left(\frac{36kT\tau}{\pi et_o G_o W\Delta\rho} \right)^{1/3} \quad (23)$$

Equations 17 and 19-23 were specifically derived for the significantly retained components with $R \sim 6\lambda$. Retention relationships for both $R = 6\lambda$ and $R = 6\lambda - 12\lambda^2$ are listed in Table 1.

Retention Predictions

The expanded particle-size separation range for the τ-delayed field programming is illustrated in Figure 3. The plots show the predicted retention of polystyrene latices under typical operating conditions. TDE-SFFF clearly produces a wider log-linear separation range than simple exponential field-decay programming. The significant deviation of the latter from the desired log-linear retention relationship (dashed line) is apparent in the small particle region. As shown in the figure, the τ-delayed or TDE-SFFF plot is linear for sample components that elute at retention

TABLE 1

Particle Mass - SFFF Retention Relationships

R = 6λ Approximation	T = 6λ-12λ² Approximation
•Constant Field SFFF, $G = G_o$	
$M = \frac{6\phi}{t_o} t_R$	$M = \frac{6\phi t_R}{t_o} - \frac{3\phi t_R}{t_o}\left(1 - \sqrt{1-4\ t_o/t_R}\right)$
•Simple Exponential-Decay, SFFF, $G = G_o e^{-t/\tau}$	
$M = \frac{6\phi\tau}{t_o}(e^{t_R/\tau}-1)$	$M = \frac{6\phi\tau}{t_o}(e^{t_R/\tau}-1) - \frac{3\phi\tau}{t_o}\left[1 - \sqrt{1 - \frac{2t_o}{3\tau}\coth(t_R/2\tau)}\right]$
•Time-Delayed-Exponential-Decay SFFF, $G = G_o$ for $t \le \tau$ and $G = G_o e^{-(t-\tau)/\tau}$ for $t > \tau$	
for $t \le \tau$, $M = \frac{6\phi}{t_o} t_R$	$M = \frac{6\phi t_R}{t_o} - \frac{3\phi t_R}{t_o}\left(1 - \sqrt{1-4\ t_o/t_R}\right)$
for $t > \tau$, $M = \frac{6\phi\tau}{et_o} e^{t_R/\tau}$	$M = \frac{6\phi\tau}{et_o} e^{t_R/\tau} - \frac{3\phi\tau}{et_o} \cdot \left[1 - \sqrt{1 - \frac{2t_o}{3\tau}\left(1-e^{-2(t_R-\tau)/\tau}\right)}\right]$
where $\phi = \frac{R_o T}{G_o W(\Delta\rho/\rho_s)}$	

times longer than the τ value of the experiment. Relative to simple exponential field programming, the TDE-SFFF approach provides retention linearity over wider particle-size ranges. Thus, this mode of SFFF operation provides the basis for more accurate

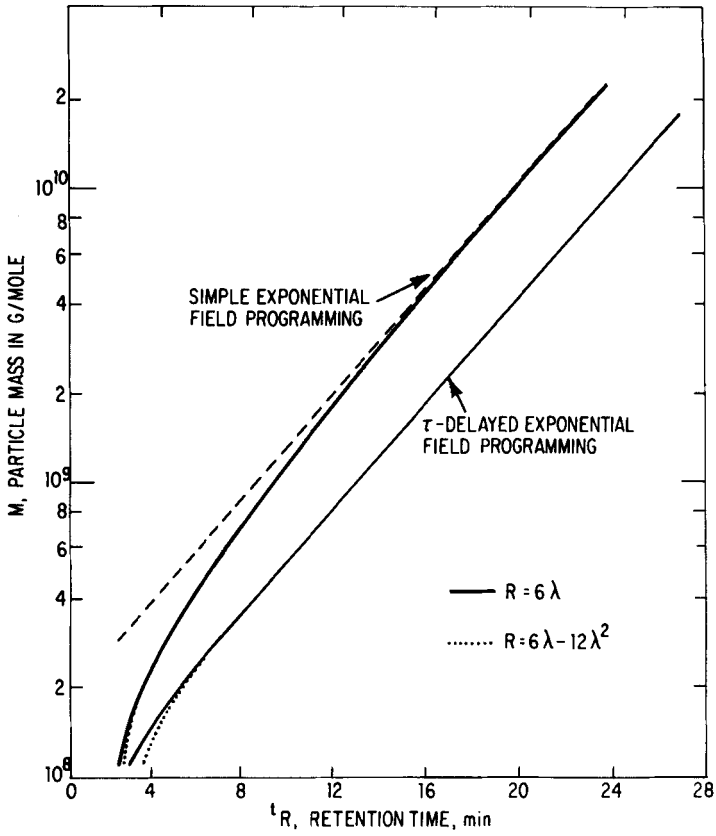

FIGURE 3. SFFF Log-Linear Retention Relationship. Data calculated by Equation (1) for: polystyrene latex standards; ρ_s, polystyrene latex, 1.05 g/cm^3; ρ_o, 0.1% FL-70 mobile phase, 1.00 g/cm^3; channel, 57 × 2.54 × 0.0125 cm; flowrate, 3.0 mL/min.; initial rotor speed, 10,000 rpm; decay time constant τ, 4.76 min.

particle size determinations. Calculated SFFF retention for the higher-order approximations of R are also plotted in Figure 3 for comparison, but the effect clearly is small.

Effect of Separation Variables

The SFFF equipment used in this study is an improved version of that described previously (4). A Digital Equipment Corp. MINC

microcomputer is interfaced with the SFFF apparatus for data reduction and control of rotor speed. In this arrangement the MINC interfaces with a Hewlett-Packard Model 59501A power supply programmer and a Model 6206B power supply to control the centrifuge motor for exponential programming. Turbidimetric detectors respond more strongly to large particles than to small particles. The MINC data handling software includes a routine for converting the uneven response of the UV-turbidimetric detector to particle size, so that true differential and cumulative particle size distribution plots can be obtained. This software package will be described in another publication.

The desirable features of TDE-SFFF have been experimentally verified, as shown in Figure 4. This fractogram of a mixture of five polystyrene latex standards was completed in about 7 minutes, with easily detected bands of approximately equal width. In Figure 5 the expected linear relation between logarithm of particle mass and t_R is shown for the data from Figure 4. Since M is proportional to d_p^3 for spherical particles, the log-linear retention relationship follows for both particle mass and particle diameter, the difference between them being a factor of three in the slope of the log-linear plots in Figure 5.

According to Equations 20 and 21, the slope of the log-linear retention relationship is only controlled by the magnitude of the τ value, the matching time-delay and exponential decay constant. Figure 6 shows the effect of the magnitude of τ values on retention and the expected slope changes of the log-linear relationship at different τ values. The plots illustrate the trade-off between analysis time and resolution by varying the exponential decay constant τ. A larger τ value causes a longer retention time but produces relatively larger spacings between the peaks for each particle size.

Other unique features of the log-linear SFFF retention relationships also can be deduced from Equations 20 and 21. According to these relationships, variations in the initial force field G_o (or ω_o), channel thickness W, mobile phase density ρ_o (or $\Delta\rho$),

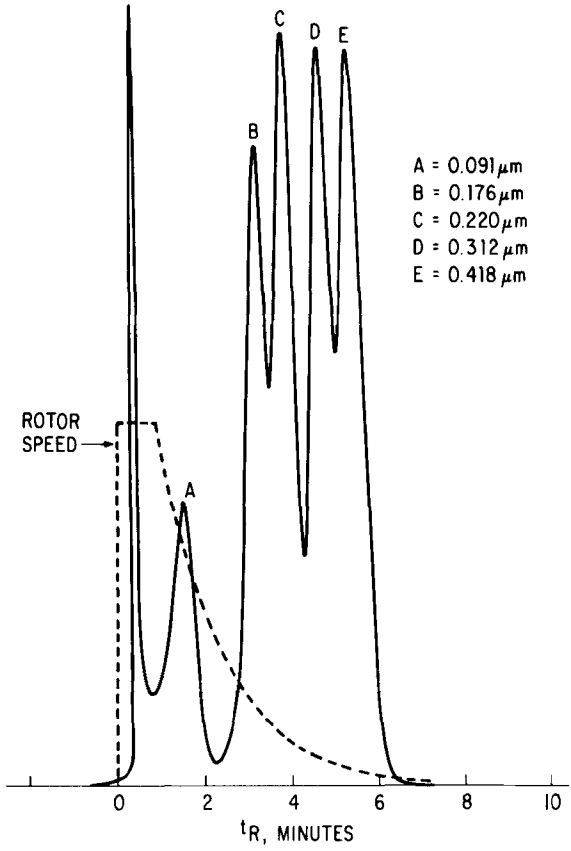

FIGURE 4. High-speed SFFF Separation of Polystyrene Latices using Time-delay Exponential Force-field Decay. Channel, 57 × 2.54 × 0.0125 cm; mobile phase, 0.1% FL 70; flowrate 7.0 mL/min.; relaxation, 1.0 min. at ω_o; initial rotor speed, ω_o, 10,000 rpm; delay and decay time constant, τ, 0.9 min; detector, UV, 254 nm; sample as in Figure 1.

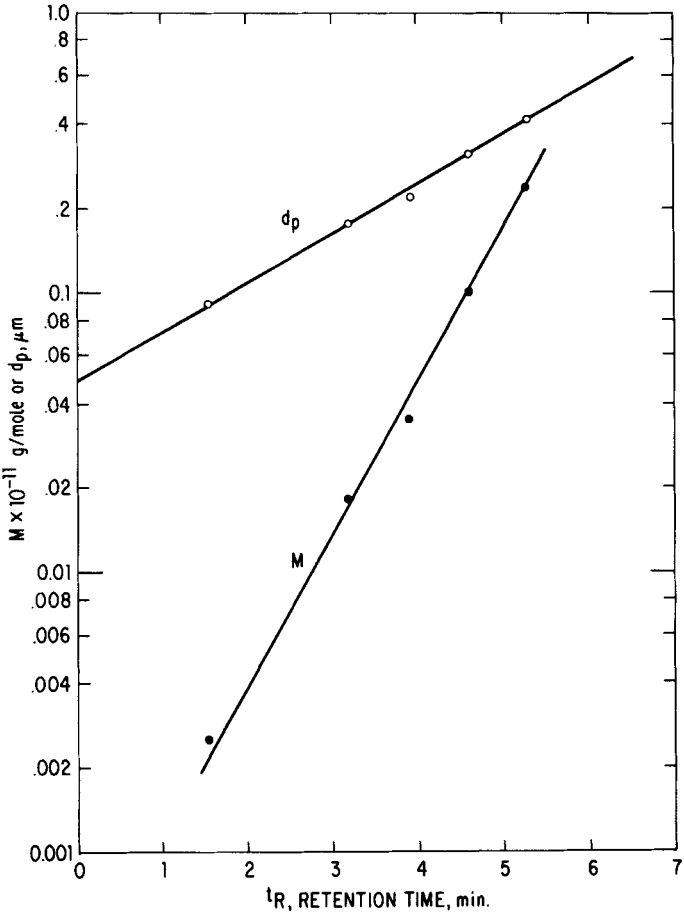

FIGURE 5. Experimental Log-Linear SFFF Retention Relationship. Data from Figure 4.

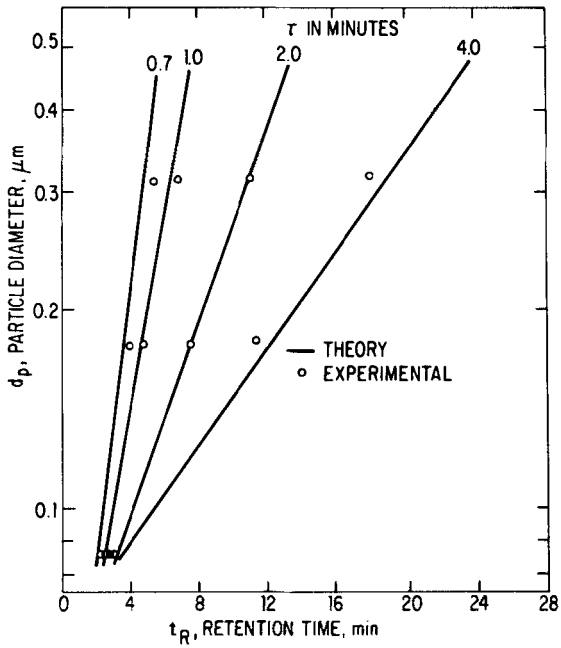

FIGURE 6. Effect of Exponential Decay Time Constant τ on SFFF Log-Linear Retention. Polystyrene standards; rest of conditions as in Figure 3, except relaxation, 1.0 min at ω_o; UV detector, 300 nm.

and flowrate F should change the intercept but not the slope of the log-linear SFFF retentionship. For example, relatively constant peak separation spacings are indicated by the plots in Figure 7 for different flowrates; the plots are parallel but displaced. Such a prediction is intuitively contradictory, but it has been substantiated experimentally. For example, the theory predicts that the retention time of sample components should be affected only modestly by flowrate differences. According to Equations 20 and 21 and the corresponding plots in Figure 7, a halving of flowrate will not double sample component retention times. Instead, all peaks are expected to elute only slightly later, with no change in relative peak separation spacings. (The theory predicts only 3.3 min. additional retention time: $\ln 2 \times \tau = 3.3$ min.). The experi-

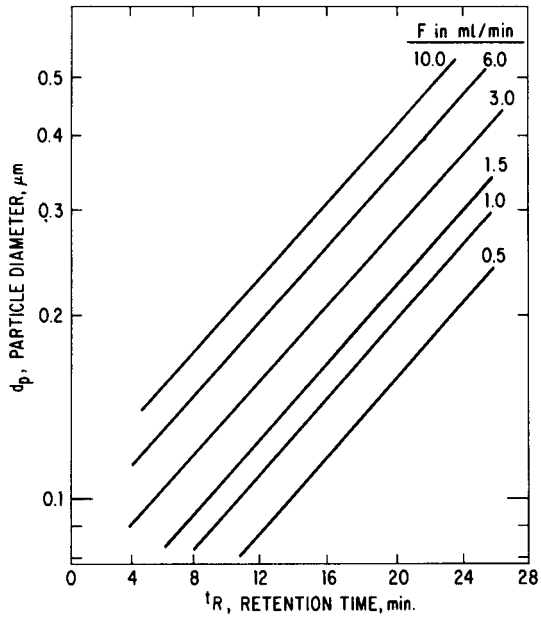

FIGURE 7. Effect of Flowrate F on Log-Linear SFFF Retention. Calculated τ-delayed data for polystyrene standards; conditions as in Figure 3, except variable flowrate.

mental conditions for separations in Figure 8 were identical except that the flowrate was halved in the lower separation, 1.5 mL/min versus 3.0 mL/min for the top curve. Note, however, that all peaks eluted in a roughly comparable time period, as predicted by theory.

There is an intuitive as well as theoretical explanation for the unusual effect of flowrate on retention as shown in Figure 8. Higher flowrates tend to elute particles faster. However, this effect in TDE-SFFF is largely negated by the higher centrifugal field being imposed at the shorter elution times. In constant-field SFFF, particle retention time is inversely proportional to flowrate, making retention volume a basic, invariant retention parameter. This is in contrast to TDE-SFFF where analyses are based more on retention time than on retention volume.

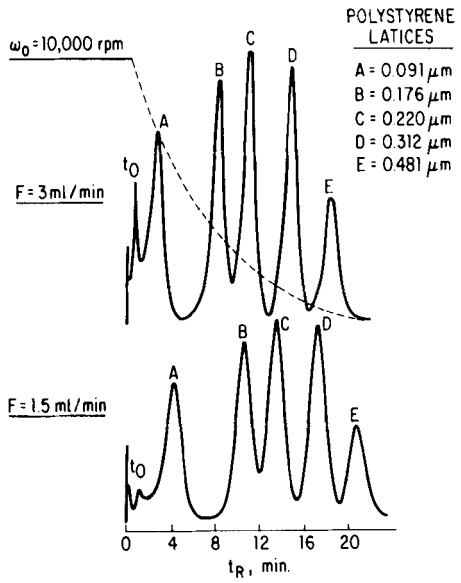

FIGURE 8. Effect of Flowrate on Exponential Field-Programmed SFFF Separation. Conditions as for Figure 3, except flowrates as shown; 10 μl of polystyrene standards: 0.09% 0.091 μm; 0.04% ea. of 0.176, 0.220 and 0.312 μm; 0.05% 0.481 μm; detector, UV, 254 nm.

The plots in Figures 9 and 10, respectively, show that changes in rotor speed ω_o and channel thickness W in TDE-SFFF affect only the intercept of the retention relationship and not the slope. Thus, increases in ω_o and W both produce greater retention of smaller particles. The unique features of the various separation parameters on the TDE-SFFF retention relationship can be utilized for carrying out convenient and rapid SFFF analyses. Plots such as those in Figures 7, 9 and 10 are handy for quickly selecting appropriate conditions to optimize separations for different particle size levels and particle size distribution ranges of interest. Retention features for TDE-SFFF, are summarized in Table 2. In particular, with TDE-SFFF, particle-size ranges can be expanded at the expense of longer analysis time by using separations of longer τ. Increase in field strength, ω_o, channel

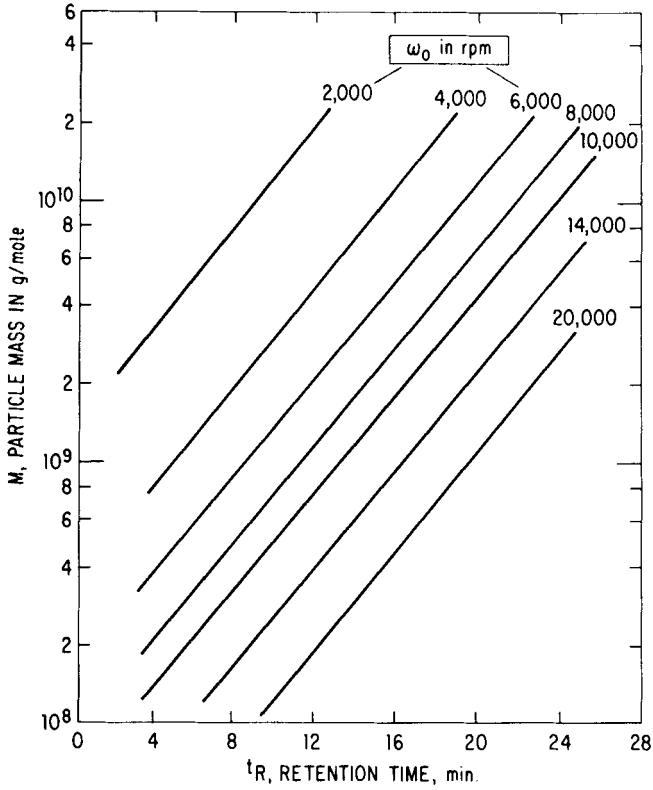

FIGURE 9. Effect of Initial Rotor Speed ω_o on Log-linear SFFF Retention. Calculated τ-delayed data for polystyrene standards; conditions as in Figure 6, except τ = 4.76 min.

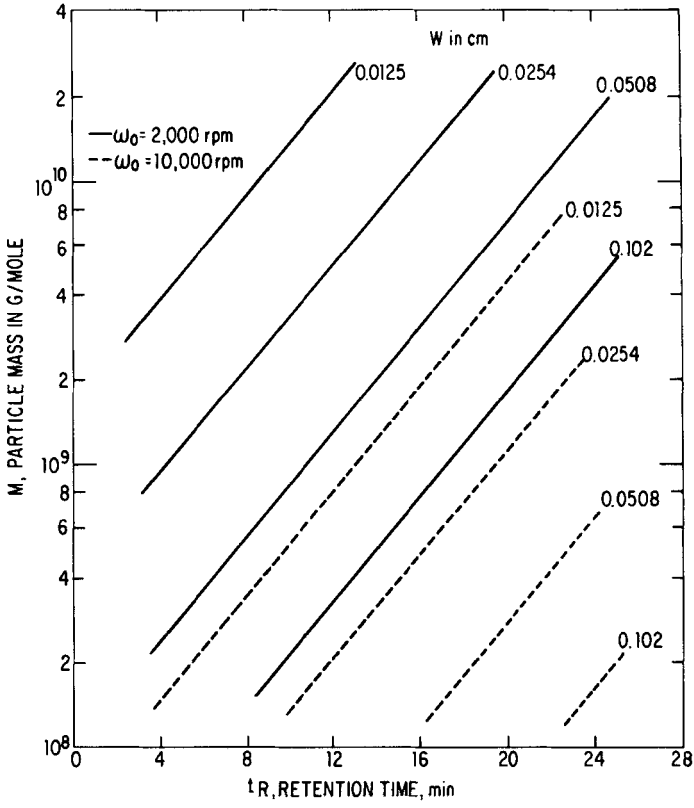

FIGURE 10. Effect of Channel Thickness W on Log-linear SFFF Retention. Calculated data for polystyrene standards; conditions as in Figure 6, except τ = 4.76 min.

dimensions, W and L, and a decrease in flowrate, F, all produce longer retention times allowing small particles to be better separated from the unretained void peak.

TABLE 2

Influence of Operating Parameters on Log-Linear Retention of τ-Delayed Exponential Field Programmed SFFF

Parameters	Slope (Particle Size Range)	Intercept (Particle Size Level)
Delay/decay time Constant, τ	++	-
Initial rotor speed, ω_o	-	++
Density difference, $\Delta\rho$	-	++
Channel thickness, W	-	++
Channel length, L	-	+
Flowrate, F	-	+
Temperature, T	-	-
Relaxation time	-	-

++ Large effect
+ Moderate effect
- Negligible or no effect

Particle Size Resolution and Accuracy

The fact that TDE-SFFF produces comparable instrumental band broadening for all eluted peaks, provides uniform resolution across the fractogram (e.g., Figures 4 and 8). Since the properties of log-linear retention in SFFF are identical to those of molecular weight calibration in size-exclusion chromatography (6), the same approach can be used to describe the effect of instrumental band broadening on particle size analyses with regard to resolution and accuracy in TDE-SFFF. Traditional chromatographic resolution is expressed as (5):

$$R_s = \frac{2(t_{R_2} - t_{R_1})}{w_1 + w_2} \simeq \frac{\Delta t_R}{4\sigma} \qquad (24)$$

where t_R is peak retention time and w is the chromatogram (or SFFF fractogram) peak width formed by intersection of the tangents to the curve inflection points with the baseline. Subscripts refer to solutes (or particles) 1 and 2, respectively. The peak standard deviation σ in Equation 24 is equal to w/4 and represents instrumental band braodening. In Equation 24 the σ values for peaks 1 and 2 are assumed equal because of the relatively uniform instrumental band broadening in TDE-SFFF (e.g., see Figures 4 and 8). Experimental σ values can be directly estimated from fractograms by measuring the peak widths of polystyrene latex standards with narrow particle-size distributions. For example, the higher flowrate separation in Figure 8 gives a σ value of 0.6 min., and the lower flowrate separation gives a σ of 0.8 min.

To describe how well particles of different sizes or masses are resolved in a TDE-SFFF separation, particle size and mass information from Equations 20 and 21 are combined with Equation 24 to give:

$$R_s = \frac{\tau . \Delta \ln M}{4\sigma} = \frac{3\tau . \Delta \ln d_p}{4\sigma} \qquad (25)$$

or for two molecular weights M_1, and M_2 or two particles sizes d_{p_1} and d_{p_2}:

$$R_s = \frac{\tau}{4\sigma} \cdot \ln\left(\frac{M_2}{M_1}\right) = \frac{3\tau}{4\sigma} \cdot \ln\left(\frac{d_{p_2}}{d_{p_1}}\right) \qquad (26)$$

These resolution equations can be used to describe the separation quality of specific particle component pairs. They do not, however, provide a general description of the resolving power of particular SFFF separations. In an analogous situation in SEC, this problem was overcome through the use of reduced resolution concepts for column performance (6, 8). By using a similar approach, the concepts of specific resolution factor $R_{s,2}$ and particle discrimination factor D_F for TDE-SFFF are now described.

We define the specific resolution factor $R_{s,2}$ as the level of resolution that a particular TDE-SFFF separation can achieve for particles with a 2-fold difference in size or mass. $R_{s,2}$ is used in SFFF rather than the value $R_{s,10}$ employed in SEC, because the significantly higher resolving power of SFFF requires a more stringent measure of particle resolution. ($R_{s,10}$ defines the resolution for materials with a 10-fold difference in mass (5)). By letting the ratios d_{p_2}/d_{p_1} or M_2/M_1 in Equation 26 equal 2, we obtain:

$$R_{s,2} \text{ (particle diameter)} = 0.52\tau/\sigma \tag{27a}$$

or,

$$R_{s,2} \text{ (particle mass)} = 0.17\tau/\sigma \tag{27b}$$

We define the particle discrimination factor D_F as the minimum particle diameter ratio (or minimum particle mass ratio) of particles that are separated with unit resolution in a particular SFFF separation. By letting R_s in Equation 26 equal unity and rearranging:

$$D_F \text{ (particle diameter)} = \exp(4\sigma/3\tau) \tag{28a}$$

$$D_F \text{ (particle mass)} = \exp(4\sigma/\tau) \tag{28b}$$

When instrumental band broadening is constant across the fractogram, as is the case for TDE-SFFF separations, values of $R_{s,2}$ and D_F provide a general and objective evaluation of the separation quality. A good SFFF separation is characterized by a large $R_{s,2}$ value for high resolving power and by a small D_F value that approaches unity for increasing particle discrimination capability.

With these reduced resolution parameters, the qualities of different SFFF separations can be compared objectively. Such comparisons can be made for a variety of SFFF experiments or with other particle size or chromatographic separation techniques. For example, the calculated resolution factors for the two TDE-SFFF fractograms of Figure 8 are compared in Table 3. The data show

that a significant increase in resolution is obtained by increasing flowrate. This result contradicts the usual chromatographic experience, but is clearly supported by SFFF theory. Such results also clearly show that SFFF is capable of producing $R_{s,2}$ values that are at least five times larger than those obtainable by SEC (compare with data in Chapt. 4, Ref. 5).

TABLE 3

Specific Resolution and Particle Discrimination Factors for Exponential Field Programmed SFFF (Fractograms of Figure 8)

Flowrate (ml/min.)	σ (min.)	Particle Diameter		Particle Mass	
		$R_{s,2}$	D_F	$R_{s,2}$	D_F
3	0.6	4.13	1.18	1.35	1.66
1.5	0.8	3.09	1.25	1.01	1.96

Since peak standard deviation (σ) values in TDE-SFFF are relatively constant with respect to retention time, the effect of instrumental band broadening on errors in particle size and particle mass analyses is highly predictable. Although these errors depend on particular separation conditions, their predictability is generally valid and applicable to all sample types, regardless of differences in sample particle size or particle size distribution.

Peaks in SFFF fractograms are influenced by instrumental band broadening. Because of this, the uncompensated, calculated particle diameters or particle mass values invariably contain some errors. The magnitude of this error can be expressed in terms of the relative percent of the true particle diameter or particle mass values:

$$\% \text{ error} = \left(\frac{1}{\theta} - 1\right) \cdot 100 \tag{29}$$

where θ is the instrumental band broadening correction factor defined as:

$$\bar{d}_p \text{ (true)} = \theta \bullet \bar{d}_p \text{ (calculated from fractogram)} \quad (30a)$$

$$\bar{M} \text{ (true)} = \theta \bullet \bar{M} \text{ (calculated from fractogram)} \quad (30b)$$

The magnitude of the error and the required correction factors vary for the different types of statistical averaging used in the particle diameter or particle mass calculations. However, the errors are very small, usually 1% or less. The error also varies with the type of detector used in the SFFF experiment.

Mathematical approaches to derive expressions for band broadening corrections factors have been previously developed for chromatographic separations (7,8). We have used an analogous approach to derive the TDE-SFFF band broadening correction factors listed in Table 4. (Definitions for the different types of $\bar{d}_p$ and $\bar{M}$ averages are from References 5, 7, 8, and are listed in Table 5 for convenience). In this derivation, band broadening is assumed to be symmetrical and can be approximated by a Gaussian shape function having a constant σ-value across the entire SFFF fractogram. The parameter γ in Table 4 specifies the detector type according to:

$$\text{(Detector Response)} \propto N\, d_p^{\gamma} \quad (31)$$

where N is the number of particles in the detector cell. When γ=0, the detector signal is proportional to the number of particles and independent of the particle size, as in the case for a particle-counter detector. With γ=6, Equation 31 describes the detector signal for a turbidity detector with light scattering in the Rayleigh regime. With γ=3, Equation 31 describes the detector signal from a weight-concentration-dependent detector such as a refractometer. The SFFF band broadening correction for a light-scattering detector operated in the Mie scattering regime (7) is more complicated and will be discussed in a future publication.

Corresponding errors in the calculated particle diameter and particle mass values can be predicted according to Equation 29 by using the appropriate θ correction factors. For example, band broadening errors for the SFFF separation shown in Figure 8 are tabulated in Table 6. Note that particle diameter errors caused by

TABLE 4

Instrumental Band Broadening Correction Factors (θ) for Exponential Field SFFF Using Different Detectors (Gaussian Instrumental Spreading Function)

Particle Diameter Averages		Turbidity Detector (γ=6)	Concentration Detector (γ=3)	Particle Counter (γ=0)	General Detector
Number Average	$\bar{d}_{p,N}$	$\exp(11\sigma^2/18\tau^2)$	$\exp(5\sigma^2/18\tau^2)$	$\exp(-\sigma^2/18\tau^2)$	$\exp[(2\gamma-1)\sigma^2/18\tau^2]$
Surface Average	$\bar{d}_{p,S}$	$\exp(5\sigma^2/9\tau^2)$	$\exp(2\sigma^2/9\tau^2)$	$\exp(-\sigma^2/9\tau^2)$	$\exp[(\gamma-1)\sigma^2/9\tau^2]$
Specific surface Average	$\bar{d}_{p,SS}$	$\exp(7\sigma^2/18\tau^2)$	$\exp(\sigma^2/18\tau^2)$	$\exp(-5\sigma^2/18\tau^2)$	$\exp[(2\gamma-5)\sigma^2/18\tau^2]$
Weight Average	$\bar{d}_{p,W}$	$\exp(5\sigma^2/18\tau^2)$	$\exp(-\sigma^2/18\tau^2)$	$\exp(-7\sigma^2/18\tau^2)$	$\exp[(2\gamma-7)\sigma^2/18\tau^2]$
Volume Average	$\bar{d}_{p,V}$	$\exp(\sigma^2/2\tau^2)$	$\exp(-\sigma^2/6\tau^2)$	$\exp(-\sigma^2/6\tau^2)$	$\exp[(2\gamma-3)\sigma^2/18\tau^2]$
Turbitidy Average	$\bar{d}_{p,\tau}$	$\exp(\sigma^2/6\tau^2)$	$\exp(-\sigma^2/6\tau^2)$	$\exp(-\sigma^2/2\tau^2)$	$\exp[(2\gamma-9)\sigma^2/18\tau^2]$
Z-Average	$\bar{d}_{p,Z}$	$\exp(-\sigma^2/18\tau^2)$	$\exp(-7\sigma^2/18\tau^2)$	$\exp(-13\sigma^2/18\tau^2)$	$\exp[(2\gamma-13)\sigma^2/18\tau^2]$
Particle Mass Averages					
Number Average	$\bar{M}_N$	$\exp(3\sigma^2/2\tau^2)$	$\exp(\sigma^2/2\tau^2)$	$\exp(-\sigma^2/2\tau^2)$	$\exp[(2\gamma-3)\sigma^2/6\tau^2]$
Weight Average	$\bar{M}_W$	$\exp(\sigma^2/2\tau^2)$	$\exp(-\sigma^2/2\tau^2)$	$\exp(-3\sigma^2/2\tau^2)$	$\exp[(2\gamma-9)\sigma^2/6\tau^2]$
Z-Average	$\bar{M}_Z$	$\exp(-\sigma^2/2\tau^2)$	$\exp(-3\sigma^2/2\tau^2)$	$\exp(-5\sigma^2/2\tau^2)$	$\exp[(2\gamma-15)\sigma^2/6\tau^2]$

TABLE 5

Definitions for Different Types of Statistical Averaging of Particle Diameter or Molecular Weight Distributions

Particle Diameter Averages		
Number Average	$\bar{d}_{p,N}$	$\Sigma\, n_i\, d_{p,i} / \Sigma\, n_i$
Surface Average	$\bar{d}_{p,S}$	$(\Sigma\, n_i\, d_{p,i}^2 / \Sigma\, n_i)^{1/2}$
Specific Surface Average	$\bar{d}_{p,SS}$	$\Sigma\, n_i\, d_{p,i}^3 / \Sigma\, n_i\, d_{p,i}^2$
Weight Average	$\bar{d}_{p,W}$	$\Sigma\, n_i\, d_{p,i}^4 / \Sigma\, n_i\, d_{p,i}^3$
Volume Average	$\bar{d}_{p,V}$	$(\Sigma\, n_i\, d_{p,i}^3 / \Sigma\, n_i)^{1/3}$
Turbidity Average	$\bar{d}_{p,\tau}$	$(\Sigma\, n_i\, d_{p,i}^6 / \Sigma\, n_i\, d_{p,i}^3)^{1/3}$
Z-Average	$\bar{d}_{p,Z}$	$\Sigma\, n_i\, d_{p,i}^7 / \Sigma\, n_i\, d_{p,i}^6$
Particle Mass Averages		
Number Average	$\bar{M}_N$	$\Sigma\, n_i\, M_i / \Sigma\, n_i$
Weight Average	$\bar{M}_W$	$\Sigma\, n_i\, M_i^2 / \Sigma\, n_i\, M_i$
Z-Average	$\bar{M}_Z$	$\Sigma\, n_i\, M_i^3 / \Sigma\, n_i\, M_i^2$

Note: n_i = Number of sample components having particle diameter $d_{p,i}$ or particle mass M_i

Σ = Sum over i for all sample components of different particle sizes (i = 1, 2, 3, ... etc.)

instrumental band broadening in this typical SFFF separation are only about 1% or less, as might be anticipated as a result of the high resolution capability of SFFF. Smaller errors are found with the higher flowrate experiment in Table 6, indicating that in exponential-field SFFF, higher flowrates produce higher resolution.

It should be noted that the peaks in the higher flowrate separation in Figure 8 appear sharper on a retention-time scale; however, they are actually broader on a retention-volume scale.

TABLE 6

Particle Diameter and Particle Mass Due to Instrumental Band Broadening for Exponential Field Programmed SFFF (Data from Figure 8; τ = 4.76 min)

			% Errors	
		0 in Eq. 29 % error = $(1/\theta-1)\cdot 100$	F=3ml/min (σ=0.6min)	F=1.5ml/min (σ=0.8 min)
Particle Diameter Averages				
Number Average	$\bar{d}_{p,N}$	$\exp(+11\sigma^2/18\tau^2)$	-0.97	-1.71
Surface Average	$\bar{d}_{p,S}$	$\exp(+5\sigma^2/9\tau^2)$	-0.88	-1.56
Specific Surface Average	$\bar{d}_{p,SS}$	$\exp(+7\sigma^2/18\tau^2)$	-0.62	-1.09
Weight Average	$\bar{d}_{p,W}$	$\exp(+5\sigma^2/18\tau^2)$	-0.44	-0.78
Volume Average	$\bar{d}_{p,V}$	$\exp(+\sigma^2/2\tau^2)$	-0.79	-1.40
Turbidity Average	$\bar{d}_{p,\tau}$	$\exp(+\sigma^2/6\tau^2)$	-0.26	-0.47
Z-Average	$\bar{d}_{p,Z}$	$\exp(-\sigma^2/18\tau^2)$	+0.09	+0.16
Particle Mass Averages				
Number Average	$\bar{M}_N$	$\exp(+3\sigma^2/2\tau^2)$	-2.36	-4.15
Weight Average	$\bar{M}_W$	$\exp(+\sigma^2/2\tau^2)$	-0.79	-1.40
Z-Average	$\bar{M}_Z$	$\exp(-\sigma^2/2\tau^2)$	+0.80	+1.42

Thus, at higher flowrates the particle concentration in peaks is less than that at the lower flowrates because of band dispersion. Eventually, detector response at low particle concentration can limit how high a flowrate one can use to improve separation resolution in exponential-field SFFF.

When a turbidity detector is used, SFFF band broadening causes negative errors, that is, the calculations underestimate particle size. Table 6 shows that the particle diameter values calculated from the SFFF fractogram in Figure 8 are less than the expected

true values, except as predicted for the high-order Z-average in $\bar{d}_{p,Z}$. The errors are, however, insignificantly small.

The accuracy and reproducibility of TDE-SFFF particle size analyses will be reported in a forthcoming publication.

ACKNOWLEDGMENTS

It is a pleasure to thank Charles H. Dilks, Jr. for his skilled assistance with the experimental work and his helpful suggestions during this study. The cooperation of J. Clarence Fogg and William A. Doerner with various mechanical developments is also greatly appreciated. We appreciate the critical review of this manuscript by D.D. Bly.

REFERENCES

1. F.J.F. Yang, M.N. Myers, and J.C. Giddings, Anal. Chem. 46, 1924 (1974).

2. F.J.F. Yang, M.N. Myers, J.C. Giddings, J. Colloid and Interface Sci. 60, 574 (1977).

3. J.C. Giddings, L.K. Smith and M.N. Myers, Anal. Chem. 48, 1587 (1976).

4. J.J. Kirkland, W.W. Yau, W.A. Doerner and J.W. Grant, Anal. Chem. 52, 1944 (1980).

5. W.W. Yau, J.J. Kirkland and D.D. Bly, Modern Size-Exclusion Liquid Chromatography, Wiley-Interscience, New York, 1979, Chapters 4, 9 and 10.

6. W.W. Yau, J.J. Kirkland, D.D.Bly and H.J. Stoklosa, J. Chromatogr. 125, 219 (1976).

7. A.E. Hamielec and S. Singh, J. Liq. Chromatogr. 1, 187 (1978).

8. A. Husain, A.E. Hamielec and J. Vlachopoulos in ACS Symposium Series, T. Provder, ed., Washington, D.C., 1980.

9. E. Pfannkoch, K.C. Lu, F.E. Regnier, and H.G. Barth, J. Chromatogr. Sci. 18, 430 (1980).

Given in part at the American Chemical Society Analytical Chemistry Award Symposium, Houston, Texas, March 23, 1980.